arXiv:1309.5460v1 [physics.space-ph] 21 Sep 2013

Effective recombination coefficient and solar zenith angle effects on low-latitude D-region ionosphere evaluated from VLF signal amplitude and its time delay during X-ray solar flares

Tamal Basak • Sandip K. Chakrabarti[1]

Abstract Excess solar X-ray radiation during solar flares causes an enhancement of ionization in the ionospheric D-region and hence affects sub-ionospherically propagating VLF signal amplitude and phase. VLF signal amplitude perturbation ($\triangle A$) and amplitude time delay ($\triangle t$) (vis-á-vis corresponding X-ray light curve as measured by GOES-15) of NWC/19.8 kHz signal have been computed for solar flares which is detected by us during Jan-Sep 2011. The signal is recorded by SoftPAL facility of IERC/ICSP, Sitapur (22° 27′N, 87° 45′E), West Bengal, India. In first part of the work, using the well known LWPC technique, we simulated the flare induced excess lower ionospheric electron density by amplitude perturbation method. Unperturbed D-region electron density is also obtained from simulation and compared with IRI-model results. Using these simulation results and time delay as key parameters, we calculate the effective electron recombination coefficient (α_{eff}) at solar flare peak region. Our results match with the same obtained by other established models. In the second part, we dealt with the solar zenith angle effect on D-region during flares. We relate this VLF data with the solar X-ray data. We find that the peak of the VLF amplitude occurs later than the time of the X-ray peak for each flare. We investigate this so-called time delay ($\triangle t$). For the C-class flares we find that there is a direct correspondence between $\triangle t$ of a solar flare and the average solar zenith angle Z over the signal propagation path at flare occurrence time. Now for deeper analysis, we compute the $\triangle t$ for different local diurnal time slots DT. We find that while the time delay is anti-correlated with the flare peak energy flux ϕ_{max} independent of these time slots, the goodness of fit, as measured by *reduced*-χ^2, actually worsens as the day progresses. The variation of the Z dependence of *reduced*-χ^2 seems to follow the variation of standard deviation of Z along the T_x-R_x propagation path. In other words, for the flares having almost constant Z over the path a tighter anti-correlation between $\triangle t$ and ϕ_{max} was observed.

Keywords X-ray solar flare, time delay, recombination coefficients, D-region ionosphere

1 Introduction

The ionosphere of the earth is a gigantic detector and it characteristically responds to the ionizing agents of terrestrial and extra-terrestrial origin. In particular, it is long known that the hard and soft X-rays originating from solar flares (Mitra 1974; Pant 1993) and strong compact celestial sources like X-ray novae, galactic centre do perturb the lower ionospheric D-region (Sharma et al. 1972; Kasturirangan et al. 1976). The excess EUV and X-ray radiations produced during the solar flares cause excess ionization (Basak et al. 2010; Garcia-Rigo et al. 2007; Chakrabarti et al. 2012). This manifests in an enhancement of the free electron density of the D-region by several orders of magnitude than the normal value. This is primarily due to the electron detachment from nitrogen and oxygen (Thomson and Clilverd 2001). The main physical mechanism behind the ionospheric effects of the solar flares have been discussed by Mitra (1974). A comparative study between the changes of VLF signal amplitude (and phase) and solar X-ray flux has been made by several workers such as Ananthakrishnan et al. (1973) and Pant (1993).

Tamal Basak

Sandip K. Chakrabarti

S. N. Bose National Centre for Basic Sciences, Block-JD, Sector-III, Salt Lake, Kolkata- 700098, India

[1]Indian Centre for Space Physics, 43 Chalantika, Garia Station Road, Garia, Kolkata- 700084, India

Through some recombining electron loss processes, mainly, the electron-ion recombination, ion-ion recombination and three body recombination, the ionosphere gradually comes back to its normal condition. In the present paper, we analyse VLF signal data coming from NWC/19.8 kHz and recorded at Ionospheric and Earthquake Research Centre (IERC) of Indian Centre for Space Physics (ICSP), at Sitapur (22° 27′N, 87° 45′E), India. The T_x-R_x *Great Circular Path* is 5691kms long and average signal attenuation along this path is low. We present the VLF response along with the corresponding X-ray flux of the solar flares which were detected during Jan-Sep 2011 and studied the evolution of recombination of the D-region during several classes of flares. VLF amplitude time delay ($\triangle t$) and electron density (N_e) are used as key parameters to obtain the recombination coefficient α_{eff}.

To handle D-region chemistry at lower heights ($\sim$ 70 km) Mitra and Rowe (1972) prescribed a 6-ion + electron scheme, where the ions are O_2^-, NO^+, O_2^+, O_4^+, $H^+(H_2O)_n$ and $NO_3^-(H_2O)_n$. After studying all reaction channels Mitra and Rowe (1972) showed that, at those lower heights, even due to significant flare induced ionization, the variation of positive and hydrated ions are less. In D-region above 74-75 kms the negative ions are practically absent. There the main ion contents are NO^+ and $H_2O_5^+$. At 75 to 80 km height, the production of O_2^+ is less than NO^+ under quiet and flare X-ray conditions (Mitra and Rowe 1974). So main clustering is done with NO^+, through $NO^+ \rightarrow NO^+.CO_2 \rightarrow H^+(H_2O)_3$ (Mitra and Rowe 1972). Clustering of O_2^+ and O_4^+ are possible only during direct photo-ionization process under flare conditions. But a large fraction of hydrates are lost as they go back to O_2^+ and NO_2^+. Thus under flare conditions [H_2O] and [O] varies, and as ionization rates go up the percentage of hydrate ion goes down with α_{eff}. For IERC-NWC low-latitude propagation path this chemistry is significant even at 74 km as it is evident from our results regarding α_{eff}.

Early studies of the recombination of electrons and ions in lower ionosphere were made by Appleton (1953); Mitra and Jones (1953); Mitra (1974). Subsequently, in a series of papers, from the ionospheric data obtained from rocket measurements and other experiments and using the electron continuity theory, the dissociative recombination coefficient (α_D), mutual ionic recombination coefficient (α_i), electron to negative ion ratio (λ) etc. are estimated and modelled (Whitten and Poppoff 1961; Poppoff and Whitten 1962; Whitten and Poppoff 1962). Mitra (1963) has reported different methods to estimate recombination coefficients (including height profile) at different ionospheric conditions, e.g., diurnal asymmetry method, eclipse method and solar decay curve method. Values of α_i and α_D obtained by the above mentioned methods agree with the experimental results. Whitten et al. (1965); Parthasarathy and Rai (1965); Gledhill (1986) have developed theoretical methods for empirical expressions for α_{eff} (it includes α_i, α_D, λ and other dust capture coefficients of aerosol theory). Wagner and Thome (1972) proposed a different method namely 'Thomson Scatter Experimental Technique' to simulate electron density and α_{eff} during solar flares relative to pre-flare condition at E-region. According to Appleton (1953), the N_e and α_{eff} are directly related to time delay $\triangle t$. This $\triangle t$ appears due to 'inertial' properties and chemical reaction time scales of the D-region ionosphere. This time delay is defined as,

$$\triangle t = APT - FPT, \tag{1}$$

where, APT is the Amplitude Peak Time of VLF signal and FPT is the X-ray Flare Peak Time. This $\triangle t$ is nearly similar to the *sluggishness* (Appleton 1953; Valnicek et al. 1972) and *relaxation time* (Mitra 1974). Balachandra Swamy (1991) has analysed photo-ionization rates in detail for different ion constituents (NO^+,O_2^+) and for different solar X-ray bands. Hence assuming photo-chemical equilibrium, the height profile of α_{eff} for different M and X classes of flares has been computed. In last few years, the calculation of the recombination coefficients for different types of solar and geomagnetic events have been done. Pozo et al. (1997) estimated α_{eff} of nighttime auroral ionosphere using EISCAT radar data and showed clearly that α_{eff} is greatly decreased with the increase in particle precipitation flux at higher energy. The same EISCAT radar observation is used by Osepian et al. (2009) to model α_{eff} during solar proton events. To compare experimental measurements of α_{eff} with those obtained from the theory Friedrich et al. (2004) inserted temperature and pressure of lower ionosphere in α_{eff} expression empirically. Using two different approaches of D-region electron continuity theory, workers such as Zigman et al. (2007) calculated α_{eff} during the flare peak and Nina et al. (2011) during the decay regime of a flare.

In the later section of the paper we analysed the zenith angle (Z) dependence of $\triangle t$ in greater detail. First, we compute the time delay of the response of the VLF signals with respect to all types of classes of solar X-ray flux variation. For NWC-IERC path, positive VLF amplitude change is observed for flares considered here. Similar results are also reported for NAA/24.0 kHz to Belgrade path by Zigman et al. (2007). The $\triangle$t measured for NWC-IERC path is found to be positive.

We showed that this $\triangle$t depends on the solar zenith angle at flare occurrence time along the signal propagation path.

There are several works in the literature on the changes in VLF signal amplitude and phase and the time delay have been carried out for studying D-region evolution due to solar flares. Earlier theoretical works on ionospheric changes were done by Wait (1962), Wait and Spies (1964), Mitra (1974) etc. Thomson and Clilverd (2001),McRae and Thomson (2004) and Thomson et al. (2005) probed the D-region changes during flares through the VLF amplitude analysis. In a review, Tsurutani et al. (2009) discussed the long term effects on the ionosphere by solar flares followed by Fast Interplanetary Coronal Mass Ejections (ICMEs). Qian et al. (2011) showed the dependency of TEC of ionosphere on solar zenith angle. Le et al. (2007), Zhang et al. (2011), Le et al. (2012) and others reported that flare induced Total Electron Content (TEC) decreases when zenith angle increases. All these works discuss the effects of solar zenithal angle on upper and middle ionosphere.

Mitra (1974) established a relation of τ with the maximum electron density ($N_{e,max}$). Mitra (1974) showed that during a given solar flare, the 'τ' is inversely related with $N_{e,max}$, i.e., for stronger flares, the ionospheric response is more instantaneous. Similar kind of results is reported by Valnicek and Ranzinger (1972). Using the X-ray data obtained by Inter-cosmos 1 satellite, they showed that the 'sluggishness' ($\triangle t$) decreases when solar induced ionizing activity increases and vice versa. Zigman et al. (2007) calculated the time variation of N_e during several classes of flares using 'electron continuity theory' and $\triangle t$ as crucial parameter (where, VLF signal along NAA/24.0 kHz to Belgrade propagation baseline are used for analysis). Thomson and Clilverd (2001) studied both long (NLK/24.85 kHz to Dunedin, $12.3Mm$) and short (French T_x/18.3 kHz to Cambridge, $617km$) path VLF propagation. They showed that for VLF amplitude perturbation due to wide variation of Z over the path the Z-effect is less for such a long path and oppositely Z-effect is significant for shorter path. Grubor et al. (2005) monitored the VLF response during flares for a shorter path (GQD/22.1 kHz to Belgrade,$\sim$ $2000km$) and they showed that the Z-effect on amplitude and phase delay are not prominent enough but the flares occurred at higher zenith angle (i.e . during dusk and dawn) can cause amplitude and phase delay if they are strong enough. But in this paper we will analyse $\triangle t$ and its Z-effect.

In this paper, we firstly formulate a method to estimate the *effective recombination coefficient* (α_{eff}) at a low-latitude D-region ionospheric with the help of some established methods mentioned in the earlier paragraphs, where, the VLF amplitude time delay ($\triangle t$) and VLF amplitude perturbation ($\triangle A$) during a solar flare are crucial parameters. We particularly concentrated to calculate electron density because the positive and negative ions, due to their comparatively heavier masses than electron, hardly affect the VLF propagation in lower ionosphere (Mitra 1992). In the next section, we describe the way we estimate $\triangle t$ and $\triangle A$ from our VLF data. Using the well known Long Wave Propagation Capability (LWPC) code (Ferguson 1998), we simulate the maximum electron density ($N_{e,max}$) at the flare peak, where $\triangle A_{max}$ has been used as the input parameter. The 'Range Exponential' sub-program of LWPC which follows two parameter (h', β) model of lower ionosphere (Wait and Spies 1964), has been used for simulation. Finally, we use the electron continuity theory (Appleton 1953; Mitra 1963, 1974; Zigman et al. 2007) and calculate α_{eff} for all classes of flares. A good correlation has been found between α_{eff} and the peak flux of solar flare (ϕ_{max}). Moreover, the obtained values of α_{eff} by our method appear to be close to the values presented in the literature.

The second part of the work consists of two different analysis. First of which is related to Z, we studied how $\triangle t$s measured for C-class flares depend on Z computed along the propagation path during the flare occurrence time. We investigated a total of 22 flares. As the $\triangle t$ has been found to depend on the strength of flares, we chose only the C-class flares. We observe that the average zenith angle (Z) over the path during flare occurrence has a linear correlation with $\triangle$t. We compute this correlation quantitatively. Ours is an alternative method to estimate the relation between N_e-profile of D-region and Z, because $\triangle$t is directly connected to N_e (Mitra 1974; Zigman et al. 2007). Similar correlations of time delay with Z can be tested for the M-class or X-class flares but since their numbers are much lower, for a good statistics, we need to collect the data for a longer period. Now in the later part for deeper analysis, we chose 78 flares of C, M and X-classes which occurred at different diurnal times. We grouped them into six separate equal sized time bins (DT) according to their occurrence times. For each bin, we fitted $\triangle t$ versus peak flare flux (ϕ_{max}) of respective flares with an empirically chosen exponentially decaying function and calculated *reduced*-χ^2 to estimate the goodness of fit. Finally, we compute the average and standard deviation (σ) of the solar zenith angle Z (averaged over the T_x-R_x propagation path) for each DT, and the *reduced*-χ^2 varies exactly in the same way as the standard deviation (σ) of zenith angle (Z) distributed over T_x-R_x path within each time bin DT.

2 Monitoring of solar flares using VLF radio signal

For VLF amplitude measurement in this paper, we record the electric field component of NWC (19.8 kHz) transmitter signal in the units of dB above 1μV m^{-1} and with 1 s resolution. Besides, the VLF signal amplitude and phase from VTX, JJI and other transmitters are also recorded wherever available. The recording has been done by SoftPAL, a fully software version of AbsPAL (Absolute Phase and Amplitude Logger) - developed by the Radio and Space Physics Group of Otago University, New Zealand. During solar flare all VLF data are compared with solar X-ray data taken in the $0.1 - 0.8$ nm (ϕ in W m^{-1}) obtained from GOES-15, National Oceanic and Atmospheric Administration (NOAA), USA. The recording period of data in this paper belongs to the rising phase of Solar Cycle no. 24. We got $\triangle A$, $\triangle t$ >0 for all the recorded cases (see Table 1). Similar results are reported by Thomson and Clilverd (2001) for NLK/24.8 kHz to Dunedin, New Zealand path. Though we detected hundreds of flares during this period, but for α_{eff} analysis we sorted out 22 flares (C & M-classes) which occurred close to midday (Z mostly within 15° to 30°, see Table 1). This is because $\triangle A$, $\triangle t$ and N_e have significant dependence on Z averaged over the signal propagation path at occurrence time (Han et al. 2011). Thus we eliminated the major effects of Z and showed that α_{eff} has an inverse relation with ϕ_{max}. Though the ionospheric relaxation time (τ) is an intrinsic characteristics of D-region but α_{eff} varies with electron production rate (q). Different q values stand for different flare strengths. Through rigorous analysis Mitra and Rowe (1972) showed that as q goes higher, then percentage of hydrated cluster ions in the D-region gets lowered at faster rate and percentage of simple positive ions like [O] gets higher. Thus complex ion chemistry reduces to simpler molecular ion chemistry and as the consequence of that α_{eff} get reduced.

In Fig. 1, we present a typical diurnal variation of 19.8 kHz VLF signals recorded on the 16th Feb 2011 (a solar-active day with several solar flares at different times) and 12th Feb 2011 (a solar-quiet day). A total six solar flares of different classes are detected on the 16th Feb 2011. The sharp rise and the slow decay pattern of a typical X-ray irradiance is exhibited by the VLF signal amplitude and phase in these observations. In Fig. 2, we present a few examples of typical VLF amplitude response for X, M and C class flares in our receiver. These are superposed on the X-ray light curve (details of those flares are marked in the Figure). The general pattern of the X-ray light curve is same as the VLF amplitude.

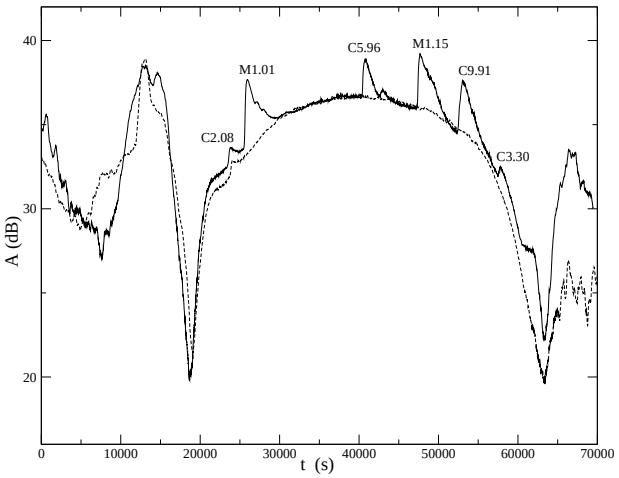


Fig. 1 The amplitude A (left) and phase (right) of VLF signals transmitted from NWC (19.8 kHz), as a function of time as recorded at IERC(ICSP), Sitapur (22° 27′N, 87° 45′E) on 16th Feb (solid line) and 12th Feb (dotted line) 2011. Six solar flares of different classes (C2.08 at 06:37 hrs, M1.01 at 07:11 hrs, C5.96 at 11:19 hrs, M1.15 at 13:14 hrs, C9.91 at 14:43 hrs and C3.3 at 16:04 hrs) were recorded on 16th Feb 2011. All times are in IST(=UT+5.5 hrs)

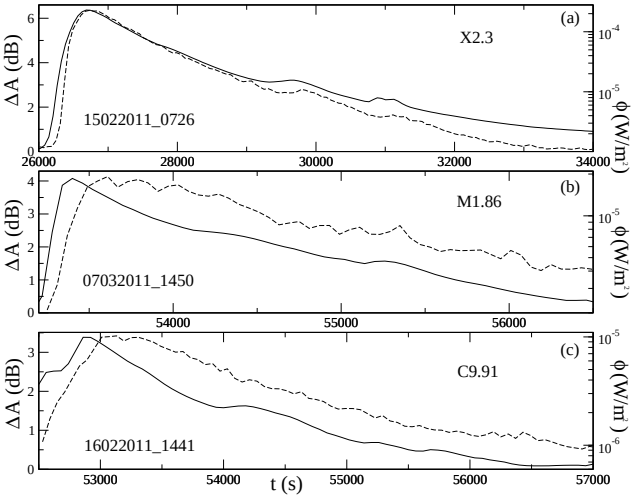


Fig. 2 Examples of (a) X-class (b) M-class and (c) C-class solar X-ray flares as recorded by GOES-15(solid lines) along with corresponding VLF signal amplitude deviations ($\triangle A$) (dashed lines). Date and time (DDMMYYYY_HHMM) are marked in respective panels.

Now to check the direct correspondence between $\triangle t$ and Z we sorted another 22 C-class flares. A total of 78 flares are of all classes are considered to estimate Z dependence of *reduced*-χ^2.

3 Estimation of $\triangle t$ and $\triangle A_{max}$

Maximum perturbed VLF amplitude ($\triangle A_{max}$) and VLF amplitude time delay ($\triangle t$) are important parameters as mentioned in the Sec. 1. These are defined as,

$$\triangle A_{max} = A_{perturbed,max} - A_{quiet}, \quad (2)$$

where, $A_{perturbed,max}$ is maximum VLF perturbation for a given solar flare and A_{quiet} is the mean of the available 5 solar-quiet day data which are closest to the 'flare day'. We have chosen solar-quiet days, such that they are free from even smaller perturbation due to tiny flares. $\triangle A_{max}$ is in dB units. Now,

$$\triangle t = t_{\triangle A_{max}} - t_{\phi_{max}}, \quad (3)$$

where, $t_{\triangle A_{max}}$ is the time of $\triangle A_{max}$ and $t_{\phi_{max}}$ is the time of peak flux (ϕ_{max}) of solar flare. Fig. 3 shows $\triangle t$ schematically. We fit the peak regions of $\triangle A$ and ϕ data sets with higher order polynomials and obtained the times at which the peaks occur. These are called $t_{\triangle A_{max}}$ and $t_{\phi_{max}}$ respectively. Overall this method reduces the error drastically. Most importantly, this fitting is important for correct estimation of $t_{\phi_{max}}$ as the maximum resolution of online available data is one minute.

This fitting method is repeated for all the flares analysed in this paper. These $\triangle A_{max}$ and $\triangle t$ are shown in Table 1 and also plotted as functions of respective ϕ_{max} in Fig. 4 and Fig. 5. In Fig. 5, we note that $\triangle t$ has a tendency of decreasing with increasing ϕ_{max}. We also find that $\triangle A_{max}$ for $\sim$ M9.0 class flare has gone up to $\sim$ 4 dB and $\triangle t$ went down to $\sim$ 70 s (see Table 1).

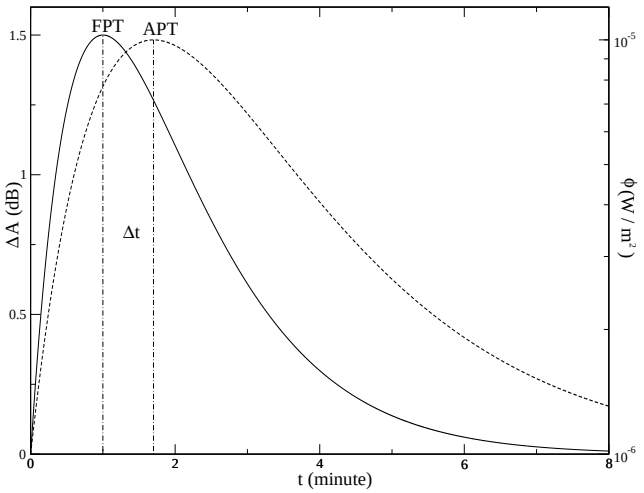


Fig. 3 A schematic diagram showing the meaning of $\triangle$t, the time delay of the VLF signal. The solid curve represents a typical soft X-ray irradiance ϕ (W/m^2) and the dashed curve represents the corresponding VLF amplitude deviation ($\triangle$A) in dB

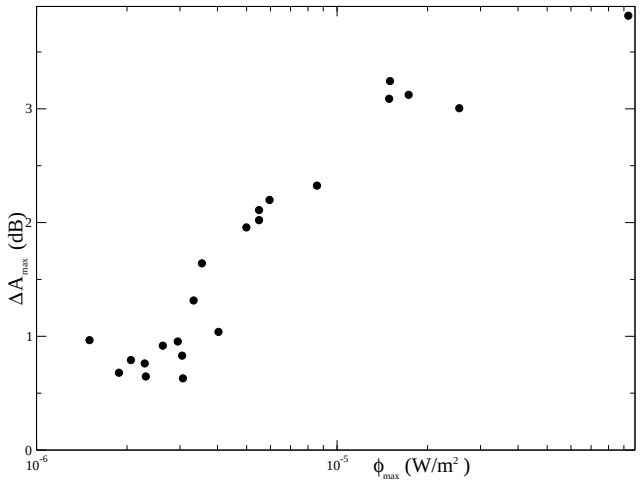


Fig. 4 Maximum perturbed VLF amplitude $\triangle A_{max}$ (in dB) is plotted as a function of corresponding peak flare flux ϕ_{max} (W m^{-2}) for all 22 flares.

4 Effective recombination coefficient during solar flares

4.1 Theoretical understanding

Our main aim in this Section is to obtain the variation of the *effective recombination coefficient* (α_{eff}) of D-region. The fundamental assumption of this calculation is that the sub-ionospheric VLF signal quickly senses the changes in D-region electron density (N_e) and modifies itself accordingly. Therefore, the VLF signal amplitude almost follows temporal variation of N_e even during flares (i.e., $t_{\triangle A_{max}} = t_{N_{e,max}}$). Keeping total charge neutrality in mind, the D-region electron continuity eqn. can be written as (Whitten and Poppoff 1961; Rowe et al. 1970),

$$\frac{dN_e}{dt} = \frac{q(t)}{1+\lambda} - \frac{N_e}{1+\lambda}\frac{d\lambda}{dt} - [\lambda^2\alpha_i + \lambda(\alpha_i+\alpha_D) + \alpha_D]{N_e}^2, \quad (4)$$

where, α_i is the ion-ion recombination coefficient, α_D is the dissociative recombination coefficient and λ is the ratio of negative ion and electron density. The electron production rate of the D-region due to $\phi(t)$ during the flare is given by (Zigman et al. 2007),

$$q(t) = \frac{C\phi(t)}{eH}\cos\chi, \quad (5)$$

where, $e = 2.71828$, $C = \rho^{-1}$ (ρ is the amount of energy required to create an electron-ion pair) and the scale

Table 1 Data sheet of all included flares

Date (*yyyymmdd*)	*time*(*s*) [*IST*]	ϕ_{max} (Wm^{-2})	*Flare class*	$\triangle A_{max}$ (*dB*)	$\chi(deg.)$	$\triangle t(s)$	$N_{e,max}$ (m^{-3})	α_{eff} (m^3s^{-1})
20110121	35230	3.33×10^{-6}	$C3.33$	1.315	27.0	151	5.19×10^9	9.155×10^{-13}
20110210	43560	1.88×10^{-6}	$C1.88$	0.68	28.7	353	3.34×10^9	153.44×10^{-13}
20110210	44873	2.06×10^{-6}	$C2.06$	0.791	32.4	307	3.63×10^9	23.94×10^{-13}
20110216	40526	5.96×10^{-6}	$C5.96$	2.199	20.5	222	9.71×10^9	5.319×10^{-13}
20110218	37272	4.03×10^{-6}	$C4.03$	1.039	18.0	183	4.38×10^9	27.67×10^{-13}
20110218	43365	8.57×10^{-6}	$C8.57$	2.325	26.7	147	10.84×10^9	5.523×10^{-13}
20110219	45278	2.63×10^{-6}	$C2.63$	0.918	32.4	247	3.86×10^9	23.197×10^{-13}
20110308	34140	15.0×10^{-6}	$M1.5$	3.244	24.3	121	26.65×10^9	1.752×10^{-13}
20110308	38246	5.5×10^{-6}	$C5.5$	2.021	14.2	140	8.97×10^9	5.182×10^{-13}
20110310	34052	2.95×10^{-6}	$C2.95$	0.955	24.6	264	4.06×10^9	67.33×10^{-13}
20110311	36141	5.5×10^{-6}	$C5.5$	2.11	17.9	140	9.89×10^9	4.4×10^{-13}
20110311	45175	3.05×10^{-6}	$C3.05$	0.83	29.6	181	3.70×10^9	21.175×10^{-13}
20110414	39420	4.99×10^{-6}	$C4.99$	1.957	14.3	134	8.60×10^9	5.282×10^{-13}
20110416	40071	3.55×10^{-6}	$C3.55$	1.641	14.7	150	6.45×10^9	6.542×10^{-13}
20110607	43800	25.5×10^{-6}	$M2.55$	3.005	28.8	90	18.36×10^9	5.929×10^{-13}
20110727	43760	3.07×10^{-6}	$C3.07$	0.63	26.8	179	3.270×10^9	37.65×10^{-13}
20110728	36861	2.29×10^{-6}	$C2.29$	0.761	23.2	190	3.48×10^9	14.855×10^{-13}
20110802	42542	14.9×10^{-6}	$M1.49$	3.088	22.6	128	20.57×10^9	2.626×10^{-13}
20110803	36131	17.3×10^{-6}	$M1.73$	3.123	23.8	145	23.71×10^9	2.283×10^{-13}
20110804	34017	93.1×10^{-6}	$M9.31$	3.818	29.3	74	44.5×10^9	4.835×10^{-13}
20110817	35940	2.31×10^{-6}	$C2.31$	0.647	22.1	298	3.82×10^9	29.61×10^{-13}
20110830	44009	1.5×10^{-6}	$C1.5$	0.966	24.7	241	4.06×10^9	6.832×10^{-13}

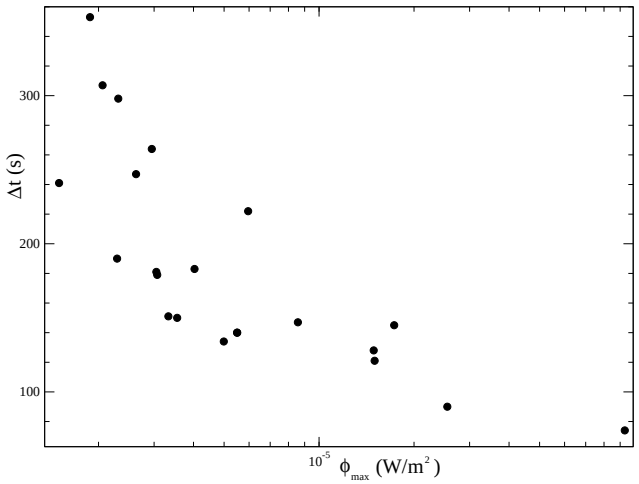


Fig. 5 VLF amplitude time delay ($\triangle t$) is plotted as a function of corresponding peak flare flux (ϕ_{max}, W m^{-2}) for the same flares showed in Fig. 4

height is given by (Mitra 1992),

$$H = \frac{k_b T}{g m_{avg}}, \tag{6}$$

where, k_b is the Boltzman constant, g is the gravitational acceleration, m_{avg} is the mean molecular mass and T is the average temperature of lower ionosphere. According to Rowe et al. (1970); Mitra (1974), λ is a slowly varying function of time. So we set, $d\lambda/dt \simeq 0$. Whitten et al. (1965); Mitra (1974) reported that, $\lambda \ll 1$ for altitudes above 70 km. So the eqn. (4) can be approximated as,

$$\frac{dN_e}{dt} = q(t) - \alpha_{eff} {N_e}^2, \tag{7}$$

where, *the effective recombination coefficient* as described in Sec. 1 is as follows,

$$\alpha_{eff} = \lambda(\alpha_i + \alpha_D) + \alpha_D. \tag{8}$$

Applying eqn. (7) near $t = t_{N_{e,max}}$ and $t_{\phi_{max}}$, the *effective recombination coefficient* would be (Zigman et al. 2007),

$$\alpha_{eff} = \frac{0.375}{\triangle t(N_{e,max} - q_{max} \triangle t)} \tag{9}$$

Comparing eqns. (5), (6) and (9) we get,

$$\alpha_{eff} = \frac{0.375}{\triangle t(N_{e,max} - \frac{\phi_{max} g m_{avg} \triangle t}{\rho e k_b T} \cos\chi)} \tag{10}$$

Among the constant terms in eqn. (10), $m_{avg} = 4.8 \times 10^{-26}$ kg (Mitra 1992) and $\rho = 34$ eV (Whitten et al.

1965). Using SROSS-C2 satellite data, Sharma et al. (2004) measured electron and ion temperature changes of ionosphere and they showed that electron temperature (T_e) changes from 1.3 to 1.9 times and ion temperature (T_i) changes from 1.2 to 1.4 times respectively during flares in comparison with normal days. Thus the change of α_{eff} due to these T_e, T_i changes is less enough compared to other ion-chemical effect induced changes. So for simplicity of the model, we justifiably assumed a thermal equilibrium and took $T = 210$ K (Schmitter 2011) to perform the entire calculation. Since only solar flares which occurred close to the mid-day have been considered in this analysis to eliminate dependence on Z, we take mean $\cos Z = 0.90$ for our calculation. This may be justified because for the flares included here, the zenith angle varies between 33° to 14° (all Z values corresponding to each flare peak time are in Table 1). Our simulation procedure to obtain $N_{e,max}$ has been discussed in the next section.

4.2 Simulation technics using LWPC

Long Wave Propagation Model (LWPM) is the default propagation model of the lower ionosphere (Ferguson 1998). It has exponential increase in N_e and conductivity. A sharpness factor (β) and effective reflection height (h') define this ionosphere model (Wait and Spies 1964). $h' = 74$ km and $\beta = 0.3$ km^{-1} are constant values being assumed to define daytime unperturbed ionosphere, even constant for entire VLF range. Here we did the simulation of lower ionosphere over the single T_x-R_x propagation path from NWC transmitter to IERC, Sitapur receiving station. As we mentioned in Sec. 4.1 that in α_{eff} analysis to avoid Z dependence, we only accommodated those flares which occurred when the sun was close to local zenith (all Z averaged over T_x-R_x path are mentioned in Table 1) w.r.t. VLF signal propagation path. So we assumed that flare induced perturbation of the reflection height for entire horizontal path segments are same.

We used Range Exponential model to handle the ionosphere perturbed due to flares. First, we have added (see Eqn. 2) the $\triangle A_{max}$ with unperturbed ionosphere VLF amplitude (A_{lwpc}) corresponding to $h' = 74$ km and $\beta = 0.3$ km^{-1} (Pal and Chakrabarti 2010; Pal et al. 2012a,b). The unperturbed D-region electron density is calculated as, $N_{e,unperturbed} = 2.2 \times 10^8 m^{-3}$. To authenticate $N_{e,unperturbed}$, we obtain the same unperturbed value (averaged over entire propagation path) from IRI-model of NASA as, $(N_{e,unperturbed})_{IRI} = 4.4 \times 10^8 m^{-3}$. There is little disagreement because LWPC follows Wait's 2-parameter lower ionospheric approximate model instead of exact realistic model. This much of disagreement of those values is justified and would not affect the physical situation as flare induced N_e is of higher magnitude than these by few orders.

Now we run the program to simulate Wait's parameters corresponding to solar flare perturbed ionosphere VLF amplitude ($A_{lwpc} + \triangle A_{max}$) and this process is repeated for all 22 flares.

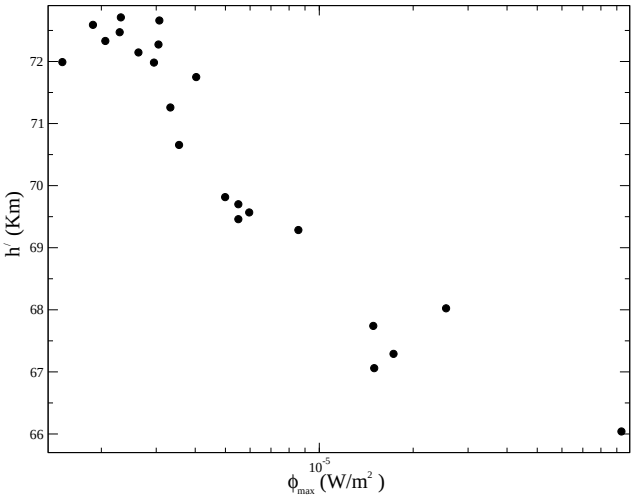


Fig. 6 Simulated effective reflection height (h') (km) is plotted with corresponding peak flare flux (ϕ_{max}) (W m^{-2})

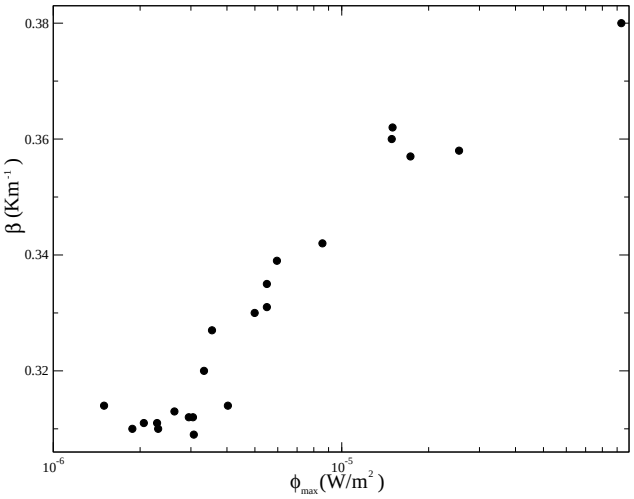


Fig. 7 Simulated sharpness factor (β) (km^{-1}) is plotted with corresponding peak flare flux (ϕ_{max}) (W m^{-2})

In Figs. 6 and 7 these h′ and β are plotted with corresponding ϕ_{max} respectively. Now using Wait's formula (Wait and Spies 1964; Pal and Chakrabarti 2010; Pal et al. 2012a,b),

$$N_{e,max} \propto e^{-\beta h'} e^{(\beta - \beta_0)h} \tag{11}$$

where, $\beta_0 = 0.15$ km^{-1}, we get electron density at height h. We repeated the entire LWPC simulation for several complex ion density profile values and we noted hardly any changes for VLF signal amplitude perturbation results. Some physical reasons in support of it, have been discussed in Sec. 1.

4.3 Results

In Sec. 4, we analysed 22 solar flares having Z within $\sim 15°$ to $30°$. We got the expression for α_{eff} as eqn. (10) and from LWPC simulation we estimated $N_{e,max}$ for each flare (eqn. 11). In Fig. 8 the LWPC simulated $N_{e,max}$ (at height $h = 74$ km) is plotted with corresponding ϕ_{max}. Also for verification of our LWPC simulation results, we again calculated $N_{e,max}$ at $h = 74.1$ km height using α_{eff} values taken from Zigman et al. (2007). Though the simulated $N_{e,max}$ values are a bit underestimated w.r.t. the values adapted from literature but the general agreement is good by keeping our measurement errors in view. Now substituting each $N_{e,max}$ to eqn. (10), α_{eff} can be calculated (see Table 1). In Fig. 9, α_{eff} versus ϕ_{max} has been shown, the values of α_{eff} goes from $\sim 10^{-13}$ m^3s^{-1} to more than 10^{-11} m^{3}s^{-1} for $\sim$ C1.0 to M9.0 classes of flares. We see that α_{eff} and ϕ_{max} are generally correlated with some exceptions. Those may have appeared due to some zenith angle (Z) variation in the observation. The calculated values of α_{eff} for low latitude D-region ionosphere generally agree with the results of Parthasarathy and Rai (1965); Balachandra Swamy (1991); Zigman et al. (2007). Fehsenfeld and Ferguson (1969); Mitra and Rowe (1972); Mitra (1974) reported that increase in solar flux intensity transforms the water-cluster ions to molecular ions. Though that process in dominant near mesopause region, but we report that at 74 km in D-region that transformation occurs at significant level and hence α_{eff} is reduced. Our results support this observation.

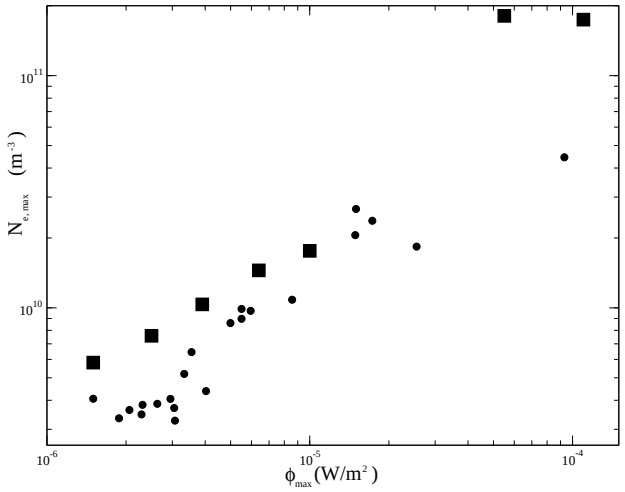


Fig. 8 (a) Simulated D-region electron density (circles) ($N_{e,max}$) (m^{-3}) at $h = 74$ km is plotted with corresponding peak flare flux (ϕ_{max}) (W m^{-2}) (b) Also $N_{e,max}$ (squares) calculated at $h = 74.1$ km using α_{eff} values taken from Zigman et al. (2007)

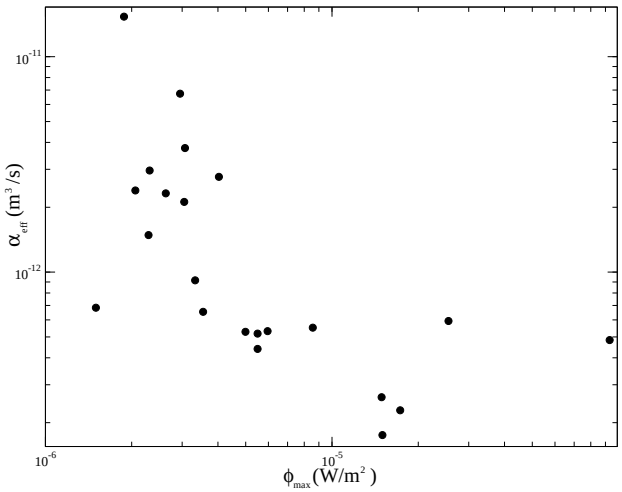


Fig. 9 *effective reflection coefficient* (α_{eff}) (m^3s^{-1}) is plotted with corresponding peak flare flux (ϕ_{max}) (W m^{-2})

5 Effects of solar zenith angle variation on flare perturbed D-region

5.1 Zenith angle effects on time delay during C-class flares

In the section we would discuss the variation of ionospheric time delay ($\triangle t$) during flare with Z over the NWC-IERC signal propagation path. We calculate the average zenith angle (Z) by taking mean of the zenith angle values at every $10km$ interval on the propagation path at the peak time of the flare. We did it to incorporate the different solar radiation inclinations at different path segments. We computed this for the 22 C-class flares which are from C2 to C7. One of the reasons to confine our discussion for a single C-class is this: the $\triangle t$ has dependence on $N_{e,max}$ and hence on ϕ_{max} according to Mitra (1974). If we mix various classes of flares, such a dependence might shadow the effect we are after. Thus we concentrated on flares of same class occurring at various times of the day. We could do similar analysis for other classes also, but the their numbers were too few to establish a correlation beyond any reasonable doubt.

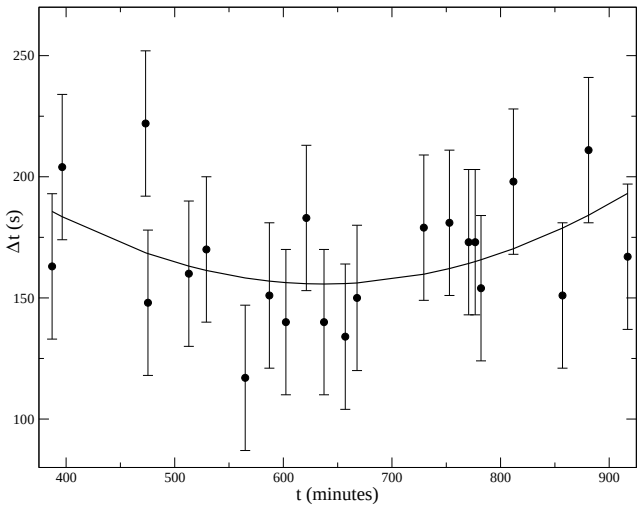


Fig. 10 The time delay ($\triangle t$) (s) of the ionosphere for each C-class solar flare is plotted as a function of their occurrence time t (mins) of the corresponding solar flare. The solid line is the fitted mean curve for those data points

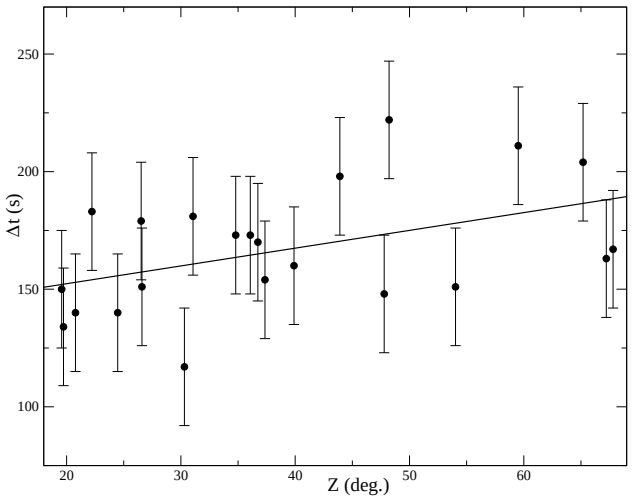


Fig. 11 The time delay ($\triangle t$) (s) of the ionosphere for each C-class solar flare is plotted as a function of Z at their occurrence time of the corresponding solar flare. The solid line is the fitted straight line for those data points

In Fig. 10, the $\triangle t$s are plotted against their occurrence time (t) [IST] and fitted curve has been drawn to actually show the variation with diurnal time and hence with Z. It is interesting that the mean curve closely follow the typical diurnal Z variation. The Z starts decreasing after sunrise. It is minimum during the mid-day when the sun is close to zenith at the top and gradually increases towards the sunset. The errorbars of $\triangle t$ represent the resolution of the recorded VLF amplitude data and the available online X-ray flux. Le et al. (2007, 2012) have shown that the Z-dependence of the upper ionosphere using TEC measurements and besides we show the Z dependence of lower ionospheric response. For further analysis, we plot the $\triangle t$ directly with corresponding Z (Fig. 11) and fitted them with a straight line to draw direct correlation. In the equation of the straight line,

$$\triangle t = a_1 Z + a_2, \tag{12}$$

The fitted values are $a_1 = 0.7556$ deg^{-1} s and $a_2 = 137.24$ s. The goodness of the fit established as the *reduced*-$\chi^2 = 0.92$ (No. of data points $N = 22$ and fitted using, $P = 2$ parameters (see eqn. 12), so the available degrees of freedom for this χ^2 - test is, $N-P = 22-2 = 20$). We see that the *reduced*-χ^2 is close to unity and thus correlation is very good. From a physical point of view this correlation can be explained in the following way: the residual degree of ionization and free electron density (N_e) of lower ionosphere is mostly governed by Z. During solar flares, bombardment of higher energetic X-ray photons on ionospheric bed leads to evolution and excitation but the Z-dependence of the flux remains.

5.2 Zenith angle dependence of correlation between ϕ_{max} and $\triangle t$

5.2.1 Grouping and analysis of solar flares

We binned 78 flares of C, M and X classes into six separate 100 *mins* sized time-bins namely, $DT1$, $DT2$, $DT3$, $DT4$, $DT5$ and $DT6$. The range of time-bins and details of flares present in those bins are given in Table 2. We chose the size of bins in a way that bins are sufficiently small so that one could assume Z to be constant in each bin, while they are sufficiently big, so that there are statistically significant number of flares in each bin. Firstly we neglected the Z variation within a given bin and secondly for validity of our statistical results we accommodated sufficient number of flare cases in each bin from available VLF data.

Time delay ($\triangle t$) is defined by eqn. (1) is similar to the time dilation parameters defined by Appleton (1953); Valnicek and Ranzinger (1972); Zigman (2007) etc. We first fitted the X-ray and VLF data analytically before obtaining $\triangle t$ (Sec. 3). In the sec. 5.1, we sorted only C-class flares and showed that, $\triangle t = f_1(Z)$, i.e., $\triangle t$s for these flares depend on mean Z computed over the signal propagation path.

While calculating α_{eff} in sec. 4, we showed that, $\triangle t = f_2(\phi_{max})$, i.e., $\triangle t$ significantly depends of the corresponding peak flare flux ϕ_{max}. In order to demonstrate, $\triangle t = f(Z, \phi_{max})$, i.e., the dependence of $\triangle t$ on ϕ_{max} and Z simultaneously, we introduce this new approach. Observing the nature of dependence we assume an empirical relation between the $\triangle t$ and ϕ_{max} for the

Table 2 Details of time-bin

	Time range (s)	C-type	M-type	X-type	a (s)	b	$Red\text{-}\chi^2$	$f = N - P$	$\sigma(deg.)$
DT1	22000-28000	6	4	1	347.0	0.39	0.923	9	3.231
DT2	28000-34000	14	3	0	247.1	0.23	1.039	15	3.084
DT3	34000-40000	8	3	0	311.3	0.35	1.324	9	6.535
DT4	40000-46000	8	2	0	346.8	0.40	1.532	8	13.698
DT5	46000-52000	11	4	1	219.4	0.29	1.663	14	12.629
DT6	52000-58000	12	1	0	238.6	0.30	1.725	11	12.26

flares in each bin:

$$\triangle t = ae^{-b(\log_{10}\phi_{max})}, \tag{13}$$

where, a and b are real parameters. Then we fitted data points of each bins separately using non-linear least square fitting technique using *Gnuplot* software and a and b are the parameter values (see Table 2) corresponding to best fitting of eqn. 13 and calculated *reduced*-χ^2 for every fit to test the 'goodness of fit'. The *reduced*-$0\chi^2$ for j-th bin is,

$$reduced - \chi_j^2 = \frac{1}{f}\sum_{DT}\frac{(\triangle t_{obs} - \triangle t_{em})^2}{\sigma_{err}^2}, \tag{14}$$

where, $\triangle t_{obs}$ is experimentally observed time delay, $\triangle t_{em}$ is the time delay calculated using eqn. 14, σ_{err} is the size of the errorbar, which comes from the limitations of the measuring instrument. In our case $\sigma_{err} = 30s$. Now the degree of freedom is defined as,

$$f = N - P \tag{15}$$

where, N is the number accommodated flares within j-th time-bin and P is number of model parameters used to fit N number of data points and here $P = 2$ from eqn. 13. Our main objectives in this paper is to check the nature of the $\triangle t$ at different Z. This is because, the residual degree of ionization (due to Lyman-α and soft X-ray) of lower ionosphere is mainly governed by Z. In Fig. 12, we plot the variation of Z along T_x-R_x. Six different graphs represent typical Z variation at midway of each time bin. Along the entire path, Z varies considerably for some time bin (e.g. $DT3$, $DT4$, $DT5$, $DT6$ mainly), and thus it is not possible to assume Z to be a constant. One way to quantify Z for each time bin, would be to measure 'how bad' the assumption of constant Z is. In other words, we would be interested in obtaining the standard deviation (σ) of Z for each time bins. This σ will thus be an estimate of variation of residual ionization due to the flare alone along T_x-R_x path. In the next Section, we would test our hypothesis that if σ is large, i.e., the variation of ionization along the path is significant, then the *reduced*-χ^2 is also going to be large, i.e., the correlation between $\triangle t$ and ϕ_{max} is also loose. The opposite should also be correct.

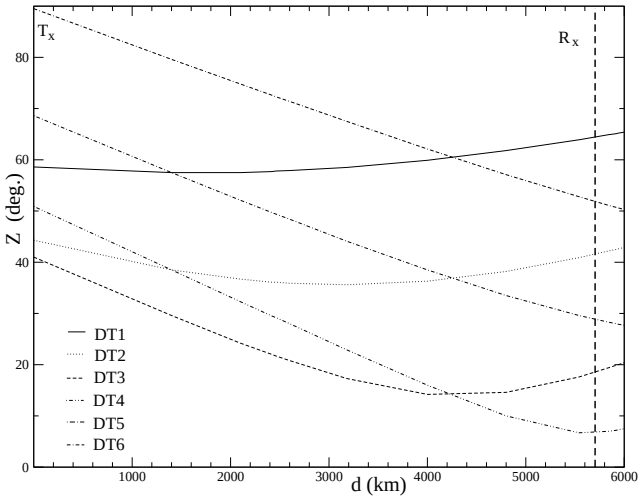


Fig. 12 Variation of mean zenith angle (Z) (deg.) as a function of T_x-R_x path at middle of time-bins mentioned in Table 2. T_x is at $d = 0km$ and R_x is at $d = 5691kms$

5.2.2 Results

We have analysed a total of 78 flares (Table 2) and for each flare, the VLF peak appeared regularly after an X-ray. Hence for all the cases under this investigation we got $\triangle t$>0. Grouping techniques and analysing procedures of flares are also discussed in earlier section.

All the flare events are plotted bin wise in Fig. 13 and Fig. 14. Error bars reflect resolutions of available GOES-15 X-ray data from NOAA archive and IERC recorded VLF data. First, we note the decreasing tendency of $\triangle t$ with increasing ϕ_{max}, which we already reported during α_{eff} for limited number of flares within small span of Z. After fitting them with the empirical function (eqn. 13) the fitting parameters a and b are evaluated (Table 2). Thereafter we calculate *reduced*-χ^2 for each fit to estimate the 'goodness of fit' (the degrees of freedom, f corresponding to those fitting are given in Table 2). The *reduced*-χ^2 physically represents the dominance of ϕ_{max} on $\triangle$t during the flares at an effective ionization level of the D-region governed by Z. Six different time bins represents discrete residual ionized states caused by different path averaged Z

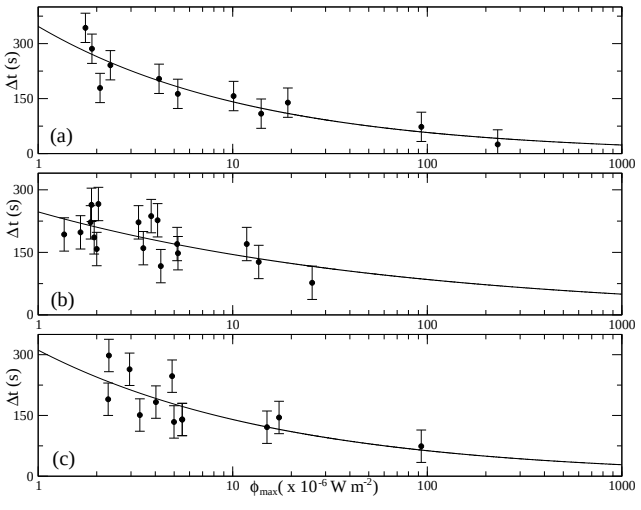


Fig. 13 The time delay ($\triangle t(s)$) for each solar flare has been plotted as a function of peak flare flux (ϕ_{max} in W m^{-2}). The solid line is the fitted empirical function (eqn. 13). The time bins are (a)$DT1$, (b)$DT2$ and (c)$DT3$

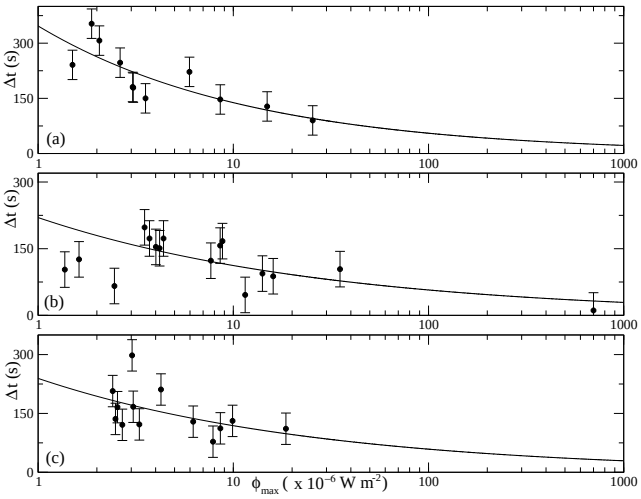


Fig. 14 The same plot of time delay ($\triangle t$) as in Fig. 13. The time bins are (a) $DT4$, (b) $DT5$ and (c) $DT6$

values. The *reduced*-χ^2 values are around 'unity' which means that the correlation is generally very good. However, as we progress from $DT1$ to $DT6$, we see that the *reduced*-χ^2 increases. Thus the fitting becomes poorer and control of ϕ_{max} over $\triangle t$ weakens gradually.

So far we discussed the physical property of $\triangle t$. Possible physical explanation of this, at least for the low-latitude, trans-equatorial, medium length signal propagation path (NWC-IERC) can be understood by the following exercise. In Fig. 12, the variation of Z over T_x-R_x path at mid-point of the time bins is very significant. This Z variation and hence the variation of residual ionization level of D-region over the propagation path increases monotonically from $DT1$ to $DT6$. The standard deviation (σ) of Z denotes the spread of it over the path (Fig. 15).

Our findings indicate that the gradient of residual ionization level over T_x-R_x path is the key determining factor of $\triangle t$ for different classes of solar X-ray flares occurred at different times.

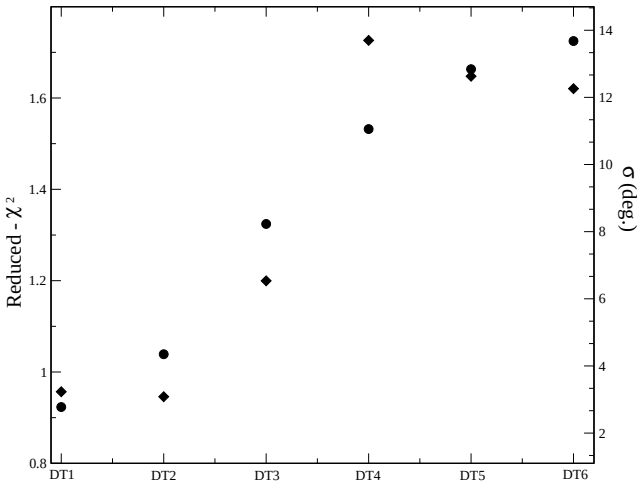


Fig. 15 The *reduced*-χ^2 (circle) and standard deviation (σ) (diamond) of the zenith angle (Z) along T_x-R_x path as functions of $DT1$, $DT2$, $DT3$ etc.

6 Conclusions

We monitored the X-ray data of GOES-15 and VLF data from NWC/19.8 kHz station as received at the IERC station by SoftPAL receiver. These data are analysed in this paper. The data acquisition period is Jan-Sep 2011. For α_{eff} calculation, we analyse VLF data of 22 flares which occur near the local mid-day in order to eliminate the effects of the Z. The signals were from NWC/19.8 kHz transmitter and are recorded at IERC/ICSP, Sitapur, India. For all the flares presented in this paper, we estimates $\triangle A$, $\triangle t > 0$. The $\triangle t$ is the important parameter in this analysis. From Fig. 5, we find a decreasing nature of $\triangle t$ with increasing ϕ_{max}. From this result, we can verify the Appleton (1953) relation regarding $\triangle t$. Most importantly we calculated the effective recombination coefficient (α_{eff}) at the peak of these flares using a coupled theoretical model which consists of electron continuity theory and LWPC simulation (Fig. 9). The values of α_{eff} at 74 km altitude are generally in agreement with earlier results reported by several other workers. The zenith angle dependence and latitude-longitude dependence have not been studied this section.

While checking direct connection between Z and $\triangle t$, we concentrated on a very narrow range of flare energies

(C2-C7) in order that the dependence of $\triangle$t on ϕ_{max} may be ignored. The most important result we reported here is the linear correlation between the solar zenith angle (Z) averaged over the propagation path at the flare time and the time delay $\triangle$t between FPT and APT for that flare. The fit is excellent as the reduced χ^2 is found to be close to unity. We believe that when we narrow our choice of flare energies even further, the correlation would be even tighter. This and a similar study for M and X-class flares would be taken up when we have data for a sufficient number of flares.

Now we moved towards a broader approach and we successfully analysed 78 flares of all classes. We generally find that the time delay of the VLF amplitude $\triangle t$ is anti-correlated with the flare energy flux ϕ_{max}. However, the relationship is not equally good. From the *reduced*-χ^2 of the fit between the $\triangle t$ and ϕ_{max}, we note that $reduced-\chi^2$ is low in the early hours of the day and it worsens as the time of the occurrence of flares progresses. To understand this behaviour we also plot the variation of zenithal angle of the sun Z along the propagation path in different time slots. Most interestingly we find that the standard deviation of Z in each slot, when plotted against the time slots, behave similarly as the variation of $reduced-\chi^2$ (Fig. 15). Though it is notable that $reduced-\chi^2$ is not following the σ for each of those DTs. But the over all increasing tendencies of those parameters with DTs are comparable. This indicates that the dispersion in the $\triangle t$ vs. ϕ_{max} relationship primarily depends on how dispersed the ionization is along the propagation path and it happens specifically on the earlier times of the day i.e. at $DT1$, $DT2$, $DT3$ and $DT4$. But for $DT5$ and $DT6$ the $reduced-\chi^2$ and σ behaves in slightly opposite manner. Dominant recombination processes in later part of the day may be the possible reason for that. In future we would verify this observation for more flare events. Moreover, confirmation of this observation for other T_x-R_x pairs would to make our result statistically more significant. We will also study the effect for a larger number of propagation paths. This will be reported elsewhere.

7 Acknowledgement

We thank S. Pal and S. K. Mondal for discussions and ICSP for allowing us to use the IERC data. Tamal Basak acknowledges a CSIR Fellowship for support.

References

Ananthakrishnan, S., Abdu, M. A., Piazza, L. R., D-region recombination coefficients and the short wavelengths x-ray flux during a solar flare, Planet. Space Sci., 21, 367-375, 1973.

Appleton, E. V., A note on the sluggishness of the ionosphere, J. Atmos. Terre. Phy., 3, 282-284, 1953.

Balachandra Swamy A. C., A new technique for estimating D-region effective recombination coefficients under different solar flare conditions, Astrophy. Space Sc., 185, 153-164, 1991.

Basak, T., Chakrabarti, S. K., Pal, S., Global effects on Ionospheric weather over the Indian subcontinent at sunrise and sunset, AIP Conf. Proc., 1286, 137-149, 2010.

Chakrabarti, S. K., Mondal, S. K., Sasmal, S., Pal, S., Basak, T., Chakrabarti, S., Bhowmick, D., Ray, S., Maji, S. K., Nandi, A., Yadav, V. K., Kotoch, T. B., Khadha, B., Giri, K., Garain, S. K., Choudhury, A. K., Partra, N. N., Iqbal, N., VLF signals in summer and winter in the Indian sub-continent using multi-station campaigns, IJP, 86(5), 323-334, 2012.

Fehsenfeld, F. C., Ferguson, E. E., Origin of water cluster inos in the D region, JGR, 74, 2217-2222, 1969.

Ferguson, J. A., Computer Programs for Assessment of Long-Wavelength Radio Communications, Version 2.0., Technical document 3030, Space and Naval Warfare Systems Center, San Diego, 1998.

Friedrich, M., Torkar, K. M., Steiner, R. J., Empirical recombination rates in the lower ionosphere, ASR, 34, 1937-1942, 2004.

Garcia-Rigo, A., Hernandez-Pajares, M., Juan, J. M., Sanz, J., Solar flare detection system based on global positioning system data: First results, Advances in Space Research, 39, 889-895, 2007.

Gledhill, J. A., The effective recombination coefficient of electrons in the ionosphere between 50 and 150 km, Radio Sc., 21(30), 399-408, 1986.

Grubor, D., Sulic, D., Zigman, V., Influence of solar X-ray flares on the earth-ionosphere waveguide, Serb. Astron. J. 171, 29-35, 2005.

Han, F., Cummer, S. A., Li, J., Lu, G., Daytime ionospheric D region sharpness derived from VLF radio atmospheric, JGR, 116, A05314, 2011.

Kasturirangan, K., Rao, U. R., Sharma, D. P., Rastogi, R. G., Chakravarty, S. C., Ionospheric effects of transient celestial X-ray and gamma-ray events, Astrophy. Space Sc., 42(1), 57-62, 1976.

Le, H., Liu, L., Chen, B., Lei, J., Yue, X., Wan, W., Modeling the responses of the middle latitude ionosphere to solar flares, Journal of Atmos. and Solar-Terr. Phy., 69, 1587-1598, 2007.

Le, H., Liu, L., Chen, Y., Wan, W., Statistical analysis of ionospheric responses to solar flares in the solar cycle 23, Journ. of Geo. Res., doi:10.1029/2012JA017934, 2012.

McRae, W. M., Thomson, N. R., Solar flare induced ionospheric D-region enhancements from VLF phase and amplitude observations, Journ. Atmos. and Sol. Terre. Phy., 66, 77-87, 2004.

Mitra, A. P., Jones, R. E., Recombination in the lower ionosphere, JGR, 50(3), 391-406, 1953.

Mitra, A. P., Recombination processes in the ionosphere, Advan. in Upper Atmos. Res., Ed. Landmark, Pergamon press, 57-87, 1963.

Mitra, A. P., Rowe, J. N., Ionospheric effects of solar flares - VI. Changes in D-region ion chemistry during solar flares, JATP, 34, 795-806, 1972.

Mitra, A. P., Rowe, J. N., Ionospheric constraints of mesospheric nitric oxide, JATP, 36, 1797-1808, 1974.

Mitra, A. P., Ionospheric effects of solar flares, D.Reidel Pub. Co., Holland, 1974.

Mitra, S. K., The upper atmosphere, The Asiatic Society, Calcutta, 1992.

Nina, A., Cadez, V., Sulic, D., Sreckovic, V., Zigman, V., Effective electron recombination coefficient in ionospheric D-region during the relaxation regime after solar flare from February 18, 2011, Nuclear Instruments and Methods in Physics Research B, 279, 106-109, 2011.

Osepian, A., Kirkwood, S., Dalin, P., Tereschenko, V., D-region electron density and effective recombination coefficients during twilight-experimental data and modelling during solar proton events, Ann. Geo., 27, 3713-3724, 2009.

Parthasarathy, R., Rai, D. B., Effective recombination coefficient in D-region, Scientific Report No. 1, Geophy. Inst. of the Univ. of Alaska, 1965.

Pal, S., Chakrabarti, S. K., Theoretical models for computing VLF wave amplitude and phase and their applications, AIP Conf. Proc., 1286, 42-60, 2010.

Pal, S., Chakrabarti, S. K., Mondal S. K., Modeling of subionospheric VLF signal perturbations associated with total solar eclipse, 2009 in Indian subcontinent, Advances in Space Research, 50, issue 2, 196-204, 2012.

Pal, S., Maji, S. K., Chakrabarti, S. K., First ever VLF monitoring of the lunar occultation of a solar flare during the 2010 annular solar eclipse and its effects on the D-region electron density profile, Planetary and Space Sc., 73, 310-317, 2012.

Poppoff, I. G., Whitten, R. C., D-Region Ionization by Solar X Rays, JGR, 67(7), 2986-2988, 1962.

Pant, P., Relation between VLF phase deviations and solar X-ray fluxes during solar flares, Astrophy. Space Sc., 209, 297-306, 1993.

Pozo, C. F. del, Hargraves, J. K., Aylward, A. D., Ion composition and effective ion recombination rate in the nighttime auroral lower ionosphere, JASTP, 59(15), 1919-1943, 1997.

Qian, L., Burns, A. G., Chamberlin, P. C., Solomon, S. C., Variability of thermosphere and ionosphere responses to solar flares, Journal of Geo. Res., 116, AI0309, 2011.

Rowe, J. N., Ferraro, A. J., Lee, H. S., Kreplin, R. W., Mitra, A. P., Observations of electron density during a solar flare, JATP, 32, 1609-1614, 1970.

Schmitter, E. D., Remote sensing planetary waves in the mid-latitude mesosphere using low frequency transmitter signals, Ann. Geo., 29, 1287-1293, 2011.

Sharma, D. P., Jain, A. K., Chakravarty, S. C., Kasturirangan, K., Ramanathan, K. R., Rao, U. R., Possibility of continuas monitoring of celestial X-ray sources through their ionization effects in the nocturnal D-region ionosphere, Astrophy. Space Sc., 17(2), 409-425, 1972.

Sharma, D. K., Rai, J., Israil, M., Subrahmanyam, P., Chopra, P., Garg, S. C., Enhancement in electron and ion temperatures due to solar flares by SROSS-C2 satellite, Ann. Geo., 22, 2047-2052, 2004.

Thomson, N. R., Clilverd, M. A., Solar flare induced ionospheric D-region enhancements from VLF amplitude observations, J. Atmos. and Terres. Phys., 63, 1729-1737, 2001.

Thomson, N. R., Rodger, C. J., Clilverd, M. A., Large solar flares and their ionospheric D region enhancements, J. Geophys. Res., 110, A06306, 2005.

Tsurutani, B. T., Verkhoglyadova, O. P., Mannucci, A. J., Lakhina, G. S., Li, G., Zank, G. P., A brief review of "solar flare effects" on the ionosphere, Radio Science, 44, RSOA17, 2009.

Valnicek, B., Ranzinger, P., X-ray emission and D-region 'sluggishness';, Bulletin of the Astronomical Institute of Czechoslovakia, 23, 318-322, 1972.

Wagner, L. S., Thome, G. D., Measurement of E-layer effective recombination coefficient during solar flares, Radio Sc., 7(4), 469-480, 1972.

Wait, J. R., Electromagnetic Waves in Stratified Media, Pergamon Press, Oxford, 1962.

Wait, J. R., Spies, K. P., Characteristics of the earth-ionosphere waveguide for VLF radio waves, NBS Tech. Note 300, 1964.

Whitten, R. C., Poppoff, I. G., A model of Solar-Flare-Induced Ionization in the D Region, JGR, 66(9), 2779-2786, 1961.

Whitten, R. C., Poppoff, I. G., Associative Detachment in the D Region, JGR, 67(3), 1183-1185, 1962.

Whitten, R. C., Poppoff, I. G., Edmonds, R. S., Berning, W. W., Effective recombination coefficients in the lower ionosphere, JGR, 70(7), 1737-1742, 1965.

Zhang, D. H., Mo, X. H., Cai, L., Zhang, W., Feng, M., Hao, Y. Q., Xiao, Z., Impact factor for the ionosphere total electron content response to solar flare irradiation, Journ. of Geo. Res., 116, A04311, 2011.

Zigman, V., Grubor, D., Sulic, D., D-region electron density evaluated from VLF amplitude time delay during X-ray solar flares, J. Atmos. and Terres. Phys., 69, 775-792, 2007.

This manuscript was prepared with the AAS LaTeX macros v5.2.